Journal of Alloys and Compounds 509 (2011) 5525–5531

Contents lists available at ScienceDirect

Journal of Alloys and Compounds

journal homepage: www.elsevier.com/locate/jallcom

Review

Bandgap engineering by substitution of S by Se in nanostructured $ZnS_{1-x}Se_x$ thin films grown by soft chemical route for nontoxic optoelectronic device applications

Harishchandra K. Sadekar[a,b], Anil Vithal Ghule[c], Ramphal Sharma[a,*]

[a] Thin Film and Nanotechnology Laboratory, Department of Physics, Dr. Babasaheb Ambedkar Marathwada University, Aurangabad 431004, Maharashtra, India
[b] Department of Physics, Arts, Commerce and Science College, Sonai 414105, Maharashtra, India
[c] Department of Nanotechnology, Dr. Babasaheb Ambedkar Marathwada University, Aurangabad 431004, Maharashtra, India

ARTICLE INFO

Article history:
Received 24 November 2010
Received in revised form 14 February 2011
Accepted 16 February 2011
Available online 23 February 2011

Keywords:
Semiconductor
Thin films
Chemical synthesis
Crystal structure
Optoelectronic property
Atomic force microscopy (AFM)

ABSTRACT

Thin films of nanostructured $ZnS_{1-x}Se_x$ with optimized growth parameters were prepared by soft chemical route on glass substrates. Ammonia free precursors were used at 80 °C constant bath temperature. The ratio of sulphur to selenium was changed continuously by changing the composition x (0–1), while atomic concentration of zinc was kept constant. Structure, composition and surface morphology of as-deposited films were characterized by X-ray diffraction (XRD), energy dispersive X-ray analysis (EDAX) and scanning electron microscopy (SEM), atomic force microscopy (AFM) respectively. XRD studies revealed that as-deposited films were nanostructured in nature with cubic zinc blended structure. It was further observed that the preferred orientations are along (1 1 1) plane and crystallite size decreased with increase in the value of x. SEM and AFM images revealed that films were uniform and pinhole free. The optical band gap (E_g) was calculated from the observed transmittance spectra by Urbach method. It was found that the band gap varied linearly from 3.71 to 2.70 eV, as composition x varies 0–1. The electrical properties' study revealed that the decrease in resistivity and increase in photosensitivity, as composition x varied 0–1. The observed interesting properties of $ZnS_{1-x}Se_x$ thin films justified their significance in optoelectronic device fabrication and applications, and as an environment friendly alternative to the commonly used toxic material such as CdS.

Contents

1. Introduction 5525
2. Experimental details 5526
3. Results and discussion 5527
   3.1. Compositional and structural study 5527
   3.2. Surface morphology and topography study 5528
   3.3. Optical properties study 5529
   3.4. Electrical properties study 5530
4. Conclusions 5531
   Acknowledgements 5531
   References 5531

1. Introduction

Wide-energy band-gap II–VI compounds are attractive because of their potential applications in nanostructured electronic and optoelectronic devices. The bulk, single crystal and polycrystalline thin films have been grown and characterized for several applications [1–4]. Polycrystalline thin films of $ZnS_{1-x}Se_x$ have been reported for different optoelectronic applications such as blue lasers and blue laser diodes [5], heterojunction nontoxic solar cells [6,7], etc. Now a days, growth and characterization of nanostructure $ZnS_{1-x}Se_x$ composite thin films have wide scope in optoelectronic device applications. Moreover, considering the industrial production and environmental protection issues, the nanostruc-

* Corresponding author. Tel.: +91 9422793173/240 2401365; fax: +91 240 2403115/3335.
E-mail addresses: rps.phy@gmail.com, ramphalsharma@yahoo.com (R. Sharma).

0925-8388/$ – see front matter © 2011 Elsevier B.V. All rights reserved.
doi:10.1016/j.jallcom.2011.02.089

Table 1
Experimental and observed elemental composition in EDAX spectra for as-deposited $ZnS_{1-x}Se_x$ thin films.

X	Composition	Initial atomic percentage in the bath (%)			Final atomic percentage in the film by EDAX analysis (%)		
		Zn	S	Se	Zn	S	Se
00	ZnS	50	50	00	52.0	48.0	00.0
0.2	$ZnS_{0.8}Se_{0.2}$	50	40	10	50.7	38.2	11.2
0.4	$ZnS_{0.6}Se_{0.4}$	50	30	20	51.3	28.4	20.2
0.6	$ZnS_{0.4}Se_{0.6}$	50	20	30	50.5	21.3	28.2
0.8	$ZnS_{0.2}Se_{0.8}$	50	10	40	51.9	09.6	38.4
1.0	ZnSe	50	00	50	53.0	00.0	47.0

tured $ZnS_{1-x}Se_x$ composite materials are the promising alternatives to the presently explored toxic materials such as CdS, window layer in photovoltaic applications. Furthermore, CdS as window material with lower band gap (2.4 eV), mostly absorbs the shorter wavelength photons contributing relatively less photocurrent in the shorter wavelength region, about 20% of the incident photons does not produce photocurrent [8]. The attractive alternate layers are also investigated which include Zn-based buffer layers. Zn-based compounds are promising and have demonstrated efficiencies close to those achieved with the conventional buffer layers such as CdS. Hence, $ZnS_{1-x}Se_x$ nanostructure thin films and their use as non toxic alternative for window layer in low cost solar cell fabrication have gained potential importance. Furthermore, electron affinity and electrical properties of these films can be tuned by changing the ratio of S to Se, which helps to enhance the blue response to the material [9].

Earlier, thin films of $ZnS_{1-x}Se_x$ have been prepared using molecular beam epitaxy [10,11], atomic layer epitaxy [12], high pressure sputtering [13], metal organic vapor epitaxy [14,15], metal organic chemical vapor deposition (MOCVD) [16], laser ablation [17], close space evaporation [6], spray pyrolysis [18], epitaxial growth [19], thermal evaporation [20], Successive Ionic Layer Adsorption and Reaction (SILLAR) [21], and soft chemical route technique [22–24], etc. ZnSe nanowires were synthesized by Sublimation Sandwich method (SSM) [25] and facile thermal vaporation method [26], Theoretical studies have also been carried out, wherein, Yu et al. [27] performed ab initio calculations of the structural, dielectric and lattice properties of ZnX (X = O, S, Se and Te). Among the galore of thin film deposition techniques, except soft chemical route, involve the use of either sophisticated instruments and/or toxic gases such as H_2S and/or H_2Se as precursors. In addition to this, soft chemical route technique is low cost, works at lower operating temperature and requires no special instrumentation. In this technique, substrates are immersed in an alkaline solution containing the chalcogenide source, the metal ions, added base and complexing agent. Furthermore, in soft chemical route technique, controlled chemical reactions play an important role during the deposition of thin films, and the rate of deposition can be controlled by adjusting the parameters like bath temperature, pH of solution, stirring rate and relative concentration of solutions in the bath.

In the present investigation, we report the simple and economic soft chemical route technique for the growth of $ZnS_{1-x}Se_x$ thin films by using ammonia free precursors. The effect of variation of sulphur to selenium ratio in the atomic composition on its structural and optoelectronic properties is studied. We used ammonia free deposition approach because ammonia is environmentally hazardous and contributes to pollution. Furthermore, it is difficult to maintain constant pH of bath solution throughout the deposition, due to which, perfect stoichiometric and pinhole free films are not possible. Typically, the $ZnS_{1-x}Se_x$ thin films were deposited using mixture of aqueous solutions of zinc sulphate, thiourea, selenium powder, sodium sulphite, trisodium citrate, triethanolamine (TEA), hydrazine hydrate, and sodium hydroxide (NaOH), where triethanolamine was used as the complexing agent and sodium hydroxide as the pH adjuster. Chaudhari et al. [22] deposited $ZnS_{1-x}Se_x$ thin films by solution growth technique, however, they used GaAs (1 1 0) substrate and zinc nitrate as the source solution of zinc ions. They observed polycrystalline thin films only above 90 °C bath temperature; while in our study crystalline thin films are achieved at 80 °C, relatively lower bath temperature.

2. Experimental details

Thin films of $ZnS_{1-x}Se_x$ were grown by soft chemical route (chemical bath technique) by using precursors of zinc (zinc sulphate), sulphur (thiourea), selenium (sodium selenosulphate) and suitable complexing agents. The deposition process is based on the slow release of Zn^{2+}, S^{2-} and Se^{2-} ions in the solution, which then condenses on the glass substrates. The deposition of $ZnS_{1-x}Se_x$ occurs when the ionic product of Zn^{2+}, S^{2-} and Se^{2-} exceed the solubility product of $ZnS_{1-x}Se_x$. Control of Zn^{2+} and Se^{2-} ions in the solution ultimately controls the rate of precipitation and hence the rate of film growth [28].

The substrates used for the deposition of $ZnS_{1-x}Se_x$ thin film were commercial microscope glass slides (Blue Star) with the size of 75 mm × 25 mm × 1.35 mm. Before deposition, the substrates were degreased in HNO_3 solution for 24 h, cleaned by commercial detergent and finally rinsed with de-ionized water and dried in air. This process is to ensure clean surface, which is essential for formation of nucleation centers, required for thin film deposition. All chemicals used in the present investigations were Loba Chem (AR grade). Aqueous solutions of 0.25 M zinc sulphate ($ZnSO_4$), 0.25 M sodium selenosulphate (Na_2SeSO_3), 0.25 M thiourea ($SC(NH_2)_2$), 0.2 M trisodium citrate, triethanolamine (TEA), 80% hydrazine hydrate and 4 M sodium hydroxide (NaOH) were used to prepare thin films. Sodium selenosulphate was prepared by refluxing 0.25 M selenium powder mixed with 1 M sodium sulphite in de-ionized water, which was heated to 80 °C for 8 h. Typically, 20 mL zinc sulphate solution was taken in a 50 mL glass beaker. Under continuous stirring, 30 drops of TEA, 5 mL NaOH and 5 drops of hydrazine hydrate solutions were added slowly. Initially, the solution was milky and turbid due to the formation of $Zn(OH)_2$ suspension. Addition of excess NaOH led to the dissolution of turbidity, making the solution clear and transparent. Then 5 mL trisodium citrate and 20 mL mixed volume of (according to the composition $x = 0$, 0.2, 0.4, 0.6, 0.8, and 1) freshly obtained sodium selenosulphate and thiourea solutions were added slowly with constant stirring and the pH of final mixture was adjusted to ~13. The same process was repeated for preparing thin-films of each composition $x = 0$, 0.2, 0.4, 0.6, 0.8, and 1.

Pre-cleaned glass substrates were inserted into the reaction mixture in the beaker standing parallel with the walls of the beaker, which was kept in constant temperature bath for 1 h at 80 °C. The following chemical reactions are involved during the deposition process:

$$(x)Na_2SeSO_3 + OH^- \rightarrow (x)HSe^- + Na_2SO_4 \quad (1)$$

$$(x)HSe^- + OH^- \rightarrow H_2O + (x)Se^- \quad (2)$$

$$(1-x)SC(NH_2)_2 + OH^- \rightarrow (1-x)HS^- + CH_2N_2 + H_2O \quad (3)$$

$$(1-x)HS^- + OH^- \rightarrow H_2O + (1-x)S^- \quad (4)$$

$$ZnSO_4 + 2NaOH + TEA \rightarrow Zn(OH)_2(TEA) + Na_2SO_4 \quad (5)$$

When NaOH and TEA are added to the Zn^{2+} salt solution, $Zn(OH)_2$ starts precipitating, which means that the solubility product (SP) of $Zn(OH)_2$ has exceeded, i.e.,

$$Zn^{2+} + 2OH^- + TEA \rightarrow Zn(OH)_2 + TEA \quad (6)$$

Further, the $Zn(OH)_2$ precipitate dissolves in excess NaOH solution to form zinc sodium hydroxide $Na_4Zn(OH)_6$ complex

$$Zn(OH)_2 + 4NaOH \rightarrow Na_4Zn(OH)_6 \quad (7)$$

$$Na_4Zn(OH)_6 \leftrightarrow 4Na^+ + HZnO_2^- + 3OH^- + H_2O \quad (8)$$

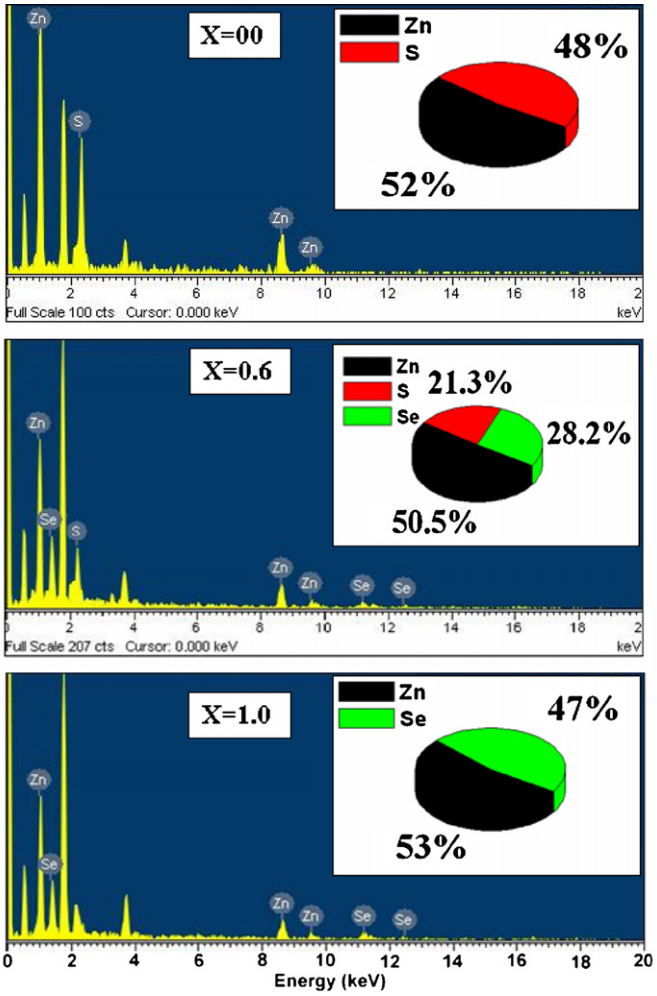

Fig. 1. Representative EDAX spectra obtained from as-deposited $ZnS_{1-x}Se_x$ thin films.

Finally, $ZnS_{1-x}Se_x$ thin film formation takes place via

$$HZnO_2^- + (x)HSe^- + (1-x)HS^- \leftrightarrow ZnS_{1-x}Se_x + 2OH^- \quad (9)$$

Thereafter, the substrate coated with $ZnS_{1-x}Se_x$ was removed, rinsed with distilled water, and dried in open air at room temperature. It was observed that the films were uniform, well adhered, and changed their color from white to reddish as x varied from 0 to 1. Thickness measured by weight difference method was found to be 260 nm. To obtain well defined diffraction peaks in X-ray diffraction (XRD), this thickness was not sufficient and thus multiple depositions were taken to obtain film thickness of about 400 nm.

Energy dispersive X-ray analysis spectra (EDAX) and scanning electron microscopy (SEM) images were obtained using JOEL-JSM 5600. The glancing incidence X-ray diffraction (GI-XRD) patterns were recorded using Bruker AXS X-ray diffractometer (Model D8 Advanced, Germany), with CuKα_1 radiation of $\lambda = 1.5406$ Å and glancing angle $\theta = 0.5^\circ$ in the detector scan mode (scan rate is 0.002) by keeping the samples fixed. Atomic force microscopy (AFM) images were obtained using Nanoscope IIIa digital instrument, Veeco Inc. in the tapping mode with a 10 nm SiC tip at room temperature and in ambient atmosphere. The optical absorption spectra were recorded on the Systronics spectrophotometer-17 within the wavelength range 300–900 nm. The DC two probe method was used for electrical resistivity measurement. Silver paste was applied for good ohmic contact with $ZnS_{1-x}Se_x$ thin films. The measurement was made in vacuum in the temperature range 340–450 K. A pico ammeter was used for current measurement.

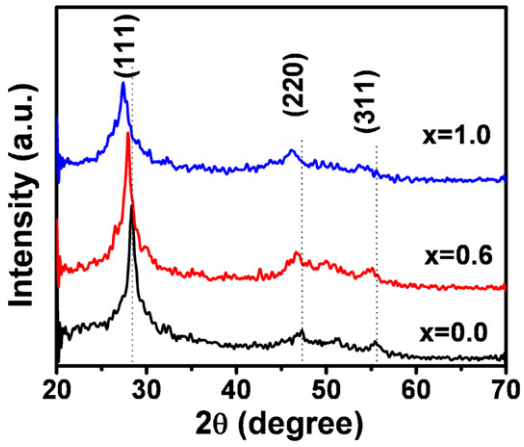

Fig. 3. Representative GI-XRD pattern obtained from the as-deposited $ZnS_{1-x}Se_x$ thin films (deposited at 80 °C bath temperature).

3. Results and discussion

3.1. Compositional and structural study

The chemical composition of the $ZnS_{1-x}Se_x$ films was confirmed by EDAX. The elemental analysis was carried out only for Zn, S, and Se, and the average atomic percentage ratio of Zn: S: Se are listed in Table 1. Fig. 1 shows representative EDAX spectra for only three compositions viz. $x = 0$, $x = 0.6$, and $x = 1.0$. It shows that the elemental composition in film is almost the same as that in the composition taken in the reaction bath mixture. The color of the films goes on changing from white to reddish as 'x' varies from 0 to 1.0 (Fig. 2). Therefore, it could be possible to grow almost stoichiometric films by solution growth technique. However, there were some additional peaks in the EDAX spectra, which could be attributed to Si, O, Ca, Mg, etc., arising due to the presence of these elements in the amorphous glass used as substrate.

Fig. 3 shows representative GI-XRD pattern of the $ZnS_{1-x}Se_x$ thin films for $x = 0$, 0.6, and 1. All the XRD patterns revealed broad peaks with (1 1 1) preferred orientation and cubic zinc blend structure. Zinc blend structure was confirmed by JCPDS card No. 77-2100

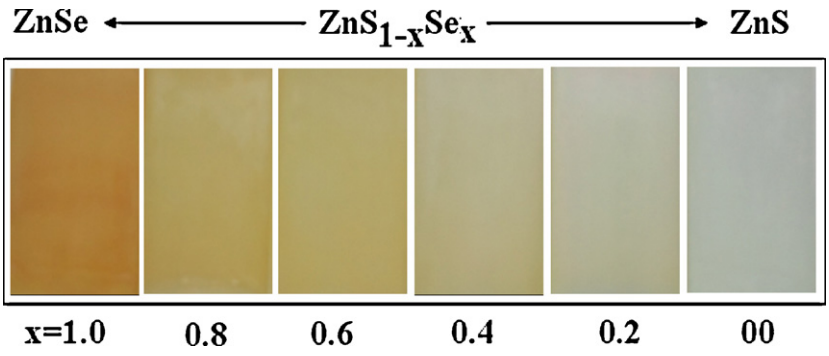

Fig. 2. Thin film images for $ZnS_{1-x}Se_x$ compositions 'x' ($0.0 \le x \le 1.0$).

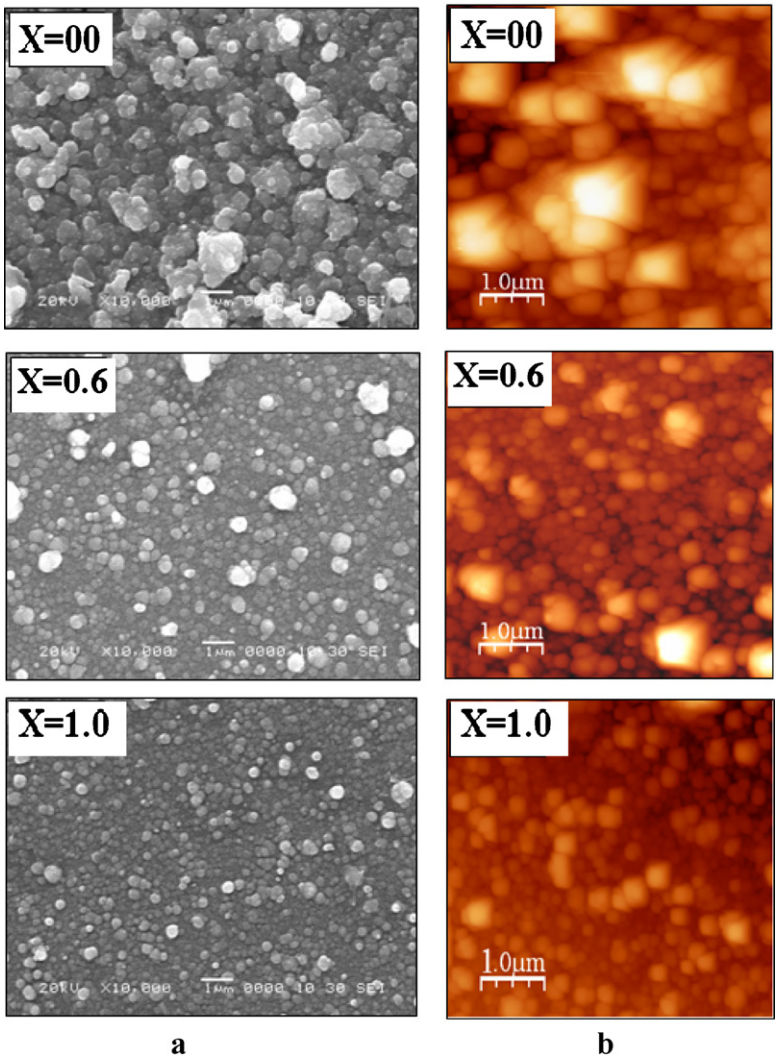

Fig. 4. Representative (a) SEM images and (b) AFM images of as-deposited $ZnS_{1-x}Se_x$ thin films.

for ZnS, and JCPDS card No. 80-0021 for ZnSe [17,29], wherein the broad peaks indicate nanostructured nature of the thin films. The shift in the peak positions towards the higher 2θ values for (1 1 1) plane (from 27.27° to 28.50°) and (2 2 0) plane (from 46.00° to 47.15°) was observed with increase of sulphur content in the films (decrease in x). This suggests that the formation of nanostructured II–VI group compounds in between ZnS and ZnSe. However, there were some other peaks present in the spectra, which can be attributed to $Zn(OH)_2$ (JCPDS card No. 71-2215). These peaks may vanish after annealing of the samples. The calculated values of the crystallite sizes by Scherrer's formula [30] using full width at half maxima (FWHM) and the lattice parameter 'a' are listed in Table 2. Crystallite size is found to decrease from 9 to 7 nm as the x value increases from 0 (ZnS) to 1 (ZnSe) i.e. towards the formation of ZnSe.

3.2. Surface morphology and topography study

Surface morphology of the films was studied by SEM. Fig. 4(a) shows representative SEM images of as-deposited ternary $ZnS_{1-x}Se_x$ thin films. It is observed that the thin films are uniform, pinhole free and cover the entire substrate surface. The fine grains were well defined, compact, and spherical with different sizes, which were uniformly distributed over the substrate without any cracks and correspond to the nanocrystalline phase of $ZnS_{1-x}Se_x$ thin films. Some of the grains were seen to be united/fused forming agglomerates in some places and the grain size obtained from SEM varies from few nanometers to 100 nm. It is also seen that the grain size increases with increase in sulphur content in the composition (i.e. decrease in x), which was confirmed by XRD study.

Table 2
Structural parameters calculated for as-deposited $ZnS_{1-x}Se_x$ thin films.

Composition	2θ (°)	d (Å)	$h\,k\,l$	a (Å)	Avg. D (nm)
ZnS	28.49	3.08	111	5.33	
	47.41	1.92	220	5.44	9.6
	56.3	1.63	311	5.15	
$ZnS_{0.8}Se_{0.2}$	28.34	3.14	111	5.44	
	47.15	1.92	220	5.43	8.8
$ZnS_{0.6}Se_{0.4}$	28.20	3.16	111	5.47	
	46.69	1.94	220	5.49	8.6
$ZnS_{0.4}Se_{0.6}$	27.84	3.2	111	5.54	
	46.39	1.95	220	5.53	8.2
$ZnS_{0.2}Se_{0.8}$	27.65	3.22	111	5.58	
	46.00	1.97	220	5.57	7.8
ZnSe	27.45	3.24	111	5.60	
	45.57	1.98	220	5.62	7.5
	54.06	1.69	311	5.61	

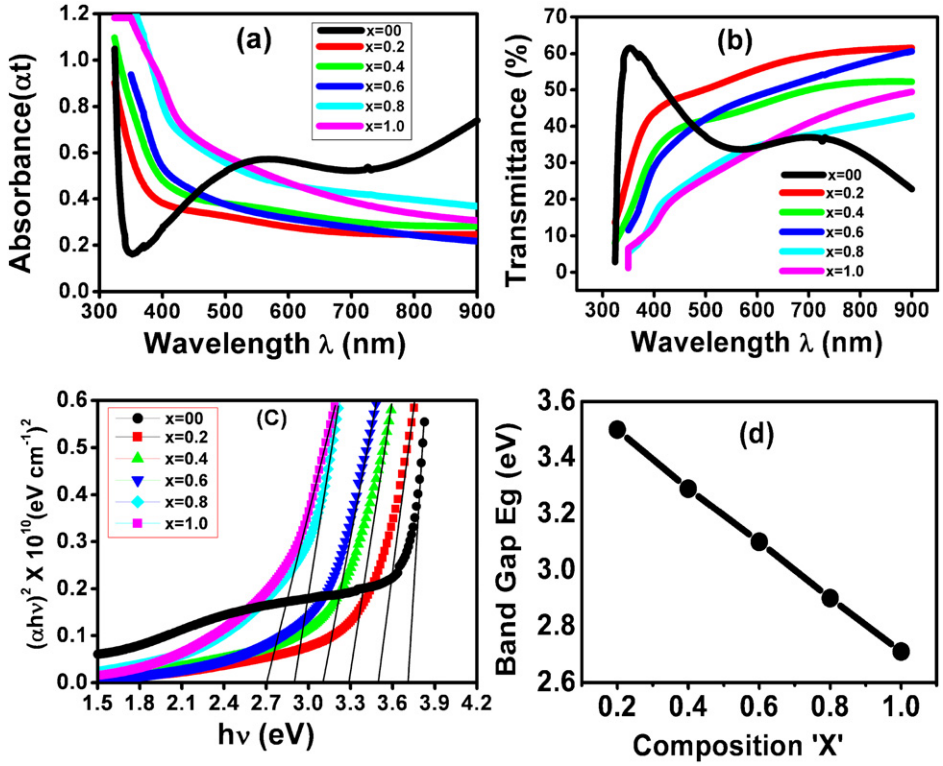

Fig. 5. (a) Plot of absorbance and (b) transmittance versus wavelength, (c) plot of $(\alpha h\nu)^2$ versus $(h\nu)$ obtained from as-deposited $ZnS_{1-x}Se_x$ thin films, and (d) variation of bandgap with change in composition x.

Particles larger than 100 nm were not observed on the surface of the films for any of the compositions with varying 'x' studied in this work. This may be attributed to the high surface energy of the small particles compared to that of the bigger ones. As a result, smaller particles tend to be deposited on the substrate, while the bigger remain in solution as $ZnS_{1-x}Se_x$ precipitate during the film growth. From the XRD and the SEM study, it is evident that there is aggregation of nanocrystallites in to grains on the substrate forming thin films. Hence, it clearly shows that the growth of $ZnS_{1-x}Se_x$ thin film takes place via cluster by cluster deposition, rather than ion by ion deposition on the surface of the substrate.

The AFM profile is used to get surface topography information of the $ZnS_{1-x}Se_x$ thin films. The atomic force microscope is ideal for quantitatively measuring the nanometer scale surface roughness and for visualizing the surface nano-texture on many types of material surfaces. Advantages of AFM for such applications are derived from the fact that AFM is nondestructive and it has a very high three dimensional spatial resolution. Fig. 4(b) shows representative two-dimensional (2-D) AFM images (5 μm × 5 μm) obtained from $ZnS_{1-x}Se_x$ thin films. The AFM topographic images show that as-deposited $ZnS_{1-x}Se_x$ film surface is uniform, pinhole free and nanocrystalline fine grains are uniformly distributed. Coagulation of small crystallites into big clusters is observed and is in good agreement with the SEM micrograph (Fig. 4(a)). The AFM images of the $ZnS_{1-x}Se_x$ films were analyzed using the software WxSm and SPIP 5.1.3. The average cluster size and surface roughness of agglomerated grains were also determined by the software and it is found that no cluster size is greater than 100 nm. The surface roughness is unavoidable because of the use of solution growth technique in this work. The results reveal that the cluster size and the granular structure with well defined grain boundaries [31] increase with increase in sulphur content in the films. The structures of the films found by SEM and AFM seem to indicate that the films grow by the aggregation of colloidal particles (nanocrystallites) formed in the solution.

3.3. Optical properties study

Fig. 5(a) and (b) show absorbance and transmittance spectra for $x = 0, 0.2, 0.4, 0.6, 0.8$, and 1 of as-deposited $ZnS_{1-x}Se_x$ thin films. The optical transmittance and absorbance spectra were used to study the optical transition in the films, which were studied at room temperature in the wavelength range of 300–900 nm. It is clearly seen from the optical spectra that the absorption edge shifts towards a longer wavelength for as-deposited thin films with increase in

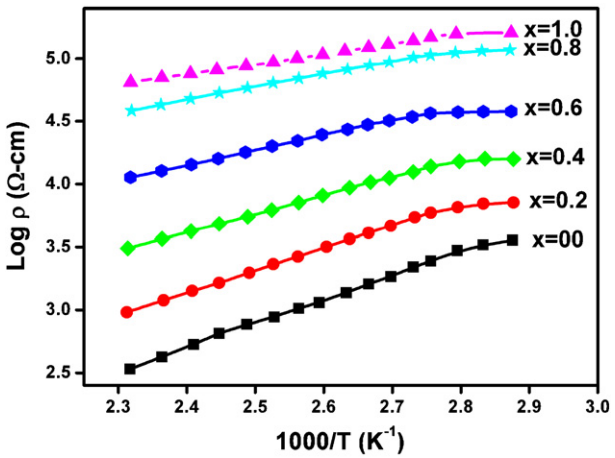

Fig. 6. Plot of $\log(\rho)$ versus $1000/T\,(K^{-1})$ obtained from as-deposited $ZnS_{1-x}Se_x$ thin films.

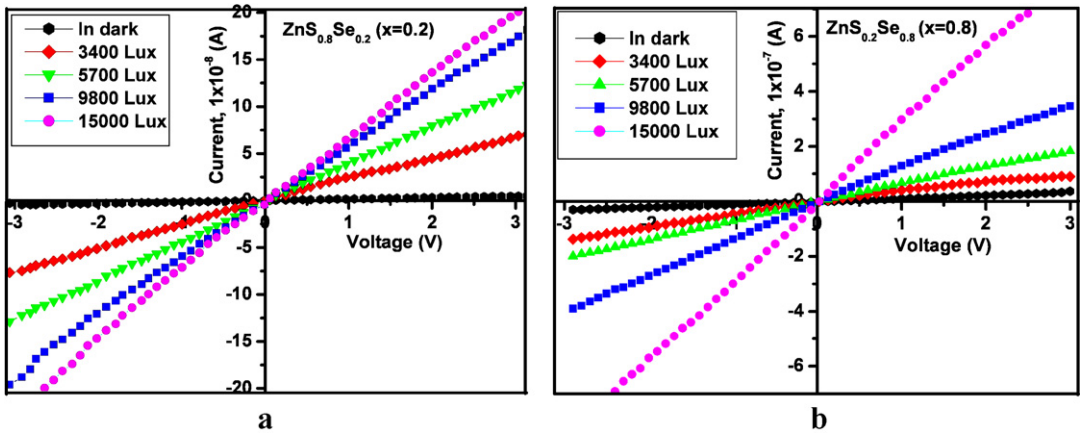

Fig. 7. Representative Current–Voltage (I–V) characteristics curve obtained from as-deposited $ZnS_{1-x}Se_x$ thin film with different illumination intensities.

composition 'x' (content of 'S' decreases). This shift gives decrease in band gap with increase in 'x'. The result also shows optical transmittance over 60% in the visible region for all the compositions. The relation between the absorption coefficient α and the incident photon energy ($h\nu$) can be expressed as (Urbach relation) [32],

$$\alpha h\nu = A(h\nu - E_g)^n \quad (10)$$

where 'A' is the constant; depending upon the transition probability for direct transition, $n = 1/2$ for direct allowed transition and 'E_g' is the optical band gap of the material. Fig. 5(c) shows the variation of $(\alpha h\nu)^2$ against $(h\nu)$ for $x = 0$, 0.2, 0.4, 0.6, 0.8, and $x = 1.0$. Extrapolating the straight-line portion of the plot of $(\alpha h\nu)^2$ versus $(h\nu)$ for zero absorption coefficient value gives the band gap, which is found to decrease from 3.71 to 2.70 eV as 'x' increases from 0 to 1. Calculated band gap energies with composition 'x' are listed in Table 3. Fig. 5(d) shows variation in band gap with variation of 'x' and demonstrates linear relationship. This implies that engineering of band gap properties of ternary $ZnS_{1-x}Se_x$ nanostructured thin films have potential applications in optoelectronic devices in wide range of solar spectrum.

3.4. Electrical properties study

The dark electrical resistivity of the thin films was measured using DC two-probe method in the temperature range from 340 to 450 K. A plot of $\log(\rho)$ versus inverse absolute temperature for cooling cycle is shown in Fig. 6. It is found that the resistivity decreases with increase in composition 'x'. The dependence is almost linear indicating the presence of only one type of conduction mechanism in the film. Our experimental data fit into the relation [33],

$$\rho = \rho_0 \exp\left(\frac{E_a}{kT}\right) \quad (11)$$

where 'ρ' is the resistivity at temperature T, 'ρ_0' is the constant, 'k' is the Boltzman's constant, 'T' is the absolute temperature and 'E_a' is the activation energy.

Table 3
Calculated band gap energy E_g and activation energy E_a for as-deposited $ZnS_{1-x}Se_x$ thin films.

X	Composition	Band gap energy E_g, eV	Activation energy E_a, eV
00	ZnS	3.71	0.37
0.2	$ZnS_{0.8}Se_{0.2}$	3.49	0.32
0.4	$ZnS_{0.6}Se_{0.4}$	3.29	0.28
0.6	$ZnS_{0.4}Se_{0.6}$	3.10	0.22
0.8	$ZnS_{0.2}Se_{0.8}$	2.89	0.18
1.0	ZnSe	2.70	0.15

The high-temperature conductivity is a thermally activated excitation of charge carriers and their mobility from nanocrystallite to nanocrystallite. In this case, activation energy was calculated from linear portion of the graph and is found to decrease from 0.37 to 0.15 eV as 'x' varies from 0 to 1. Calculated activation energies with composition 'x' are listed in Table 3. Increase in activation energy suggests that the charge carriers are trapped by the nanocrystallites, giving rise to interfacial polarization [34] and the resistivity increases. The decrease in resistivity with increase in temperature confirms the semi-conducting behavior of the films.

Fig. 7 shows representative I–V characteristics curve of as-deposited $ZnS_{1-x}Se_x$ thin films under dark and illuminated conditions. The area of $ZnS_{1-x}Se_x$ thin films (1 cm^2) on glass substrate was defined and silver paste was applied (two Ag contacts separated by a distance of 1 cm) to ensure good neutral electrical contacts to the films. The linear nature from the plot suggests the formation of ohmic contact between metal–semiconductor ($Ag/ZnS_{1-x}Se_x$) junctions, indicating that the work function of metal Ag is higher than semiconductor $ZnS_{1-x}Se_x$ films. This aligns the metal Fermi level of Ag with the upper valence band edge. The resistivity from I–V characteristics is found to decrease with increase in illumination intensity for all the compositions. It possibly might be due to the generation of electron hole pairs in the semiconductor material by incident light energy greater than the bandgap energy (E_g). This suggests that the material is photosensitive and can be used in optoelectronic device applications. It is also seen that (Fig. 7), for a given voltage (like $V = 2$ V), the current increases for compositions from $x = 0.2$ to $x = 0.8$, and is due to the decrease in electrical resistivity as composition x changes from 0 to 1. The room temperature electrical resistivity calculated by I–V in dark and with different illumination intensity are listed in Table 4 for $x = 0$–1. Resistivity of our samples is high; the reason may be the fluctuations of the inter-grain boundary region, which creates the disorder in as-deposited samples. The effects of these disorders are

Table 4
Resistivity calculated under dark and on illumination from I–V curve for as-deposited $ZnS_{1-x}Se_x$ thin films.

Composition	Resistivity, Ω cm				
	In dark	3400 lx	5700 lx	9800 lx	15000 lx
ZnS	0.86×10^9	8.67×10^8	6.54×10^8	4.36×10^8	3.89×10^8
$ZnS_{0.8}Se_{0.2}$	6.67×10^8	1.54×10^8	1.47×10^8	1.34×10^8	8.92×10^7
$ZnS_{0.6}Se_{0.4}$	2.41×10^8	4.02×10^7	2.44×10^7	1.70×10^7	1.41×10^7
$ZnS_{0.4}Se_{0.6}$	2.02×10^8	2.46×10^7	1.51×10^7	7.83×10^6	4.13×10^6
$ZnS_{0.2}Se_{0.8}$	9.26×10^7	1.49×10^7	1.01×10^7	6.25×10^6	3.53×10^6
ZnSe	3.00×10^7	9.58×10^6	7.49×10^6	6.72×10^6	4.70×10^6

reflected on the electrical conductivity by hopping of the carriers at the defect state. The resistivity might decrease by annealing.

4. Conclusions

It is possible to grow $ZnS_{1-x}Se_x$ thin films from ammonia free precursor solutions, using soft chemical route by appropriate selection of the growth parameters. As-deposited films present excellent adherence, uniform deposition of $ZnS_{1-x}Se_x$, smooth morphological and nanostructure properties, confirmed from SEM, AFM and XRD analysis. It is found that as-deposited $ZnS_{1-x}Se_x$ films are highly oriented with cubic zinc blende structure, and the preferred crystal orientations are (1 1 1) plane. The small XRD FWHM also suggests that the crystal quality of the as-deposited $ZnS_{1-x}Se_x$ films is good. The presence of $Zn(OH)_2$ is unavoidable as in case of as-deposited thin films, which can be eliminated by annealing. The EDAX study shows reasonably good stoichiometric compositions of $ZnS_{1-x}Se_x$ thin films. Energy band gap of as-deposited $ZnS_{1-x}Se_x$ films is found to vary from 3.71 to 2.70 eV as x varies 0–1. The engineering of bandgap by substitution of sulphur by selenium in $ZnS_{1-x}Se_x$ imparts interesting properties to the material, justifying its scope for potential applications in optoelectronic devices in wide range of solar spectrum. *I–V* studies reflected good photo-response of $ZnS_{1-x}Se_x$ thin films on illumination with different light intensity. The physical, optical and electrical property studies reveal that the nanostructure $ZnS_{1-x}Se_x$ thin films can be suitably employed in photosensor and/or opto-electronic applications, especially as a photovoltaic solar cell window layer, with the advantage of being the best alternative to conventionally used toxic CdS window material.

Acknowledgements

We are thankful to the Department of Physics, Dr. B.A.M. University, Aurangabad, Dr. Mrs. V.S. Rokade, Principal, Arts, Commerce and Science College, Sonai for providing laboratory facilities and for their kind cooperation. We are thankful to BCUD, University of Pune for financial support. We owe special thanks to Dr. D.M. Phase, Dr. V.R. Reddy, Dr. V. Ganesan, Dr. N.P. Lalla, Mr. Vinay Ahire, UGC-DAE, Consortium for scientific research, Indore and Dr. Fouran Singh, IUAC/NSC, New Delhi for characterization work, valuable discussions and suggestions.

References

[1] A.G. Kontos, Y.S. Raptis, M. Straßburg, U.W. Pohl, D. Bimberg, Thin Solid Films 428 (2003) 185.
[2] J.H. Jung, H.J. Kim, B.J. Kim, T.W. Kim, Y.-H. Kim, Appl. Phys. Lett. 91 (2007) 182107.
[3] F. Li, T.W. Kim, W. Dong, Y.-H. Kim, Appl. Phys. Lett. 92 (2008) 011906.
[4] X.L. Zhu, L.W. Guo, N.S. Yu, J.F. Yan, M.Z. Peng, J. Zhang, H.Q. Jia, H. Chen, J.M. Zhou, J. Cryst. Growth 306 (2007) 292.
[5] D.S. Patil, D.K. Gautam, Physica B 344 (2004) 140.
[6] Y.P. Venkata Subbaiah, P. Pratap, K.T.R. Reddy, D. Mangalaraj, K. Kim, J. Yi, J. Phys. D: Appl. Phys. 40 (2007) 3683.
[7] Y.P. Venkata Subbaiah, P. Prathap, K.T. Ramakrishna Reddy, R.W. Miles, J. Yi, Thin Solid Films 516 (2008) 7060.
[8] C. Ferekids, S. Marinskaya, D. Marinskiy, V. Palekis, D.L.S. Morel, Proceedings of the Second World Conference and Exhibition on Photovoltaic Solar Energy Conversion, Vienna, Austria, 1998.
[9] S. Fridjine, S. Touihri, K. Boubaker, M. Amlouk, J. Cryst. Growth 312 (2010) 202.
[10] K.-I. Ogata, J.J. Davies, D. Wolverson, S. Fujita, S. Fujita, Semicond. Sci. Technol. 15 (2000) 209.
[11] L.S. Lai, I.K. Sou, C.W.Y. Law, K.S. Wong, Z. Yang, G.K.L. Wong, Opt. Mater. 23 (2003) 21.
[12] C.T. Hsu, Mater. Chem. Phys. 58 (1999) 6.
[13] A. Ganguly, S. Chaudhuri, A.K. Pal, J. Phys. D: Appl. Phys. 34 (2001) 506.
[14] N. Lovergine, P. Prete, L. Tapfer, A.M. Mancini, J. Cryst. Growth 214–215 (2000) 187.
[15] A.C. Wright, N. Maung, Philos. Mag. 83 (2003) 2641.
[16] J.H. Song, E.D. Sim, K.S. Baek, S.K. Chang, J. Cryst. Growth 214–215 (2000) 460.
[17] A. Ambrico, G. Perna, D. Smaldone, C. Spezzacatena, V. Stagno, V. Capozzi, Semicond. Sci. Technol. 13 (1998) 1446.
[18] K.T. Ramakrishna Reddy, Y.V. Subbaiah, T.B.S. Reddy, D. Johnston, I. Forbes, R.W. Miles, Thin Solid Films 431–432 (2003) 340.
[19] M.-K. Lee, T.-H. Shih, B.-T. Tsay, Semicond. Sci. Technol. 18 (2003) 1030.
[20] M. Ashraf, S.M.J. Akhtar, A.F. Khan, Z. Ali, A. Qayyum, J. Alloys Compd. 509 (2011) 2414.
[21] B. Güzeldir, M. Sağlam, A. Ateş, J. Alloys Compd. 506 (2010) 388.
[22] G.N. Chaudhari, S.N. Sardesai, S.D. Sathaye, V.J. Rao, J. Mater. Sci. 27 (1992) 4647.
[23] S.R. Kang, S.W. Shin, D.S. Choi, A.V. Moholkar, J.-H. Moon, J.H. Kim, Curr. Appl. Phys. 10 (2010) S473.
[24] L. Chen, D. Zhang, G. Zhai, J. Zhang, Mater. Chem. Phys. 120 (2010) 456.
[25] H.W. Zhu, P.G. Li, M. Lei, L.H. Li, S.L. Wang, W.H. Tang, J. Alloys Compd. 509 (2011) 3306.
[26] Y. Du, Q.-X. Yuan, J. Alloys Compd. 492 (2010) 548.
[27] Y. Yu, J. Zhou, H. Han, C. Zhang, T. Cai, C. Song, T. Gao, J. Alloys Compd. 471 (2009) 492.
[28] J.M. Dona, J. Herrero, J. Electrochem. Soc. 142 (1995) 764.
[29] Y.P. Venkata Subbaiah, K.T. Ramakrishna Reddy, Mater. Chem. Phys. 92 (2005) 448.
[30] B.D. Cullity, Elements of X-ray Diffraction, 2nd ed., Addison-Wesley, Reading, MA, 1979, p. 102.
[31] S. Fridjine, K.B. Ben Mahmoud, M. Amlouk, M. Bouhafs, J. Alloys Compd. 479 (2009) 457.
[32] J. Cao, J. Yang, Y. Zhang, L. Yang, D. Wang, M. Wei, Y. Wang, Y. Liu, M. Gao, X. Liu, J. Phys. D: Appl. Phys. 43 (2010) 075403.
[33] P. Prathap, Y.P.V. Subbaiah, K.T. Ramakrishna Reddy, R.W. Miles, J. Phys. D: Appl. Phys. 40 (2007) 5275.
[34] R.P. Sharma, Indian J. Pure Appl. Phys. 35 (1997) 424.